J Mater Sci: Mater Med (2009) 20:793–798
DOI 10.1007/s10856-008-3649-1

Electrospun submicron bioactive glass fibers for bone tissue scaffold

H. Lu · T. Zhang · X. P. Wang · Q. F. Fang

Received: 26 August 2008 / Accepted: 3 November 2008 / Published online: 20 November 2008

Abstract Submicron bioactive glass fibers 70S30C (70 mol% SiO_2, 30 mol% CaO) acting as bone tissue scaffolds were fabricated by electrospinning method. The scaffold is a hierarchical pore network that consists of interconnected fibers with macropores and mesopores. The structure, morphological characterization and mechanical properties of the submicron bioactive glass fibers were studied by XRD, EDS, FIIR, SEM, N_2 gas absorption analyses and nanoindentation. The effect of the voltage on the morphology of electrospun bioactive glass fibers was investigated. It was found that decreasing the applied voltage from 19 to 7 kV can facilitate the formation of finer fibers with fewer bead defects. The hardness and Young's modulus of submicron bioactive glass fibers were measured as 0.21 and 5.5 GPa, respectively. Comparing with other bone tissue scaffolds measured by nanoindentation, the elastic modulus of the present scaffold was relatively high and close to the bone.

1 Introduction

Bone is a rigid and dynamic organ and the microstructure of bones is hierarchically patterned to provide maximal strength with minimal mass [1]. Many circumstances call for bone grafting owing to bone defects from traumatic or non-traumatic destruction [2]. Significant efforts have been made to the field of biomaterials and bone tissue engineering. An optimal scaffold for bone tissue engineering should be biocompatible, ideally osteoinductive, osteoconductive and presents similar mechanical properties compatible with the natural bone tissue [3, 4]. In addition, Hench and Polak [5] have pointed out that the third-generation biomaterials must be both bioactive and resorbent, and designed to stimulate specific cellular responses at the molecular level. The CaO–SiO_2 system is the basis for many of the third-generation tissue regeneration materials presently in development [6]. Sarvanapavan and Hench [7] have shown that in the CaO–SiO_2 system, 70S30C (70 mol% SiO_2, 30 mol% CaO) has the highest bioactivity. Jones et al. [8] have confirmed that the scaffolds made of 70S30C bioactive glass fulfill many of the criteria for an ideal scaffold applied in the field of bone tissue engineering. However, most previous researches on 70S30C bioactive glass have been restricted to the forms of powder [9], monolith [7, 10–12] or foam [3, 8, 13, 14]. A challenging study is to fabricate submicron fibrous scaffolds with defined architecture replicating the in vivo circumstance as closely as possible, which may help to maintain the phenotype and function of an in vivo like cell [15]. Submicron fibers of bioactive glass with certain composition [16, 17] had been proved to be able to improve the bioactivity and osteogenic potential.

Recently, electrospinning has been received much attention as a method to fabricate the submicron fibrous scaffolds for bone tissue engineering [18–20]. Electrospinning, a simple and versatile technique, is capable of spinning fibers with diameters down to tens of nanometers. Long, thin, solid fibers can be generated as the electrified jet (viscous solution) is continuously stretched by electrostatic forces [21]. Electrospun submicron fibers mimic the features of native extracellular matrix (ECM) and provide a niche for cell arrangement [22]. The submicron fibrous

H. Lu · T. Zhang · X. P. Wang · Q. F. Fang (✉)
Key Laboratory of Materials Physics, Institute of Solid State Physics, Chinese Academy of Sciences, Hefei 230031, People's Republic of China
e-mail: qffang@issp.ac.cn

scaffolds have significant effects on various cell behaviors including cell migration, orientation, adhesion and proliferation [15]. In comparison with other forms, the submicron fibrous form of 70S30C bioactive glass has great potential as a bone regeneration material owing to its specific shape.

In this study, the electrospinning process for the production of submicron bioactive glass fibers 70S30C was optimized. The mechanical properties of the scaffolds made of 70S30C fibers, which is necessary for the potential application in bone tissue engineering, were assessed by nanoindentation technique. The effect of the applied voltage on the defect in fibers was also investigated.

2 Experimental details

Tetraethyl orthosilicate (TEOS), calcium nitrate tetrahydrate ($Ca(NO_3)_2 \cdot 4H_2O$, 99%) and polyvinyl alcohol (PVA, average degree of polymerization: 1750 ± 50) made by Sinopharm Chemcial Reagent Co. Ltd (China) were used as precursors. Nitric acid (HNO_3, 65–68%) was used as catalyst. Initially, TEOS (0.035 mol) was added to 80 ml ethanol. After stirring for 10 h to allow complete hydrolysis of TEOS, $Ca(NO_3)_2 \cdot 4H_2O$ (0.015 mol) dissolved in ethanol was slowly dropped into the TEOS solution. Clear sol was obtained after another 2 h stirring. PVA dissolved in hot deionized water (about 90°C) was mixed with the sol, in order to adjust the viscosity to a level suitable for electrospinning (about 1 Pa s). Twenty-five ml of such hybrid solution was loaded into a plastic syringe equipped with a blunt-ended stainless steel needle (internal diameter = 1 mm), which was connected to a high-voltage power supply (the applied voltage can be adjusted between 7 and 19 kV). A syringe pump was used to control the feeding rate in a level of 0.5 ml/h. A piece of grounded flat aluminium foil was placed 15 cm away from the needle tip to collect the fibers. The as-spun submicron fibrous mat (about 1.5 mm thick) was peeled off from the aluminium foil, and then heated up to 600°C with a heating rate of 2°C/min and annealed at 600°C for 5 h in air. The annealing temperature of 600°C was chosen so that the nitrates, silanol and organic sources could be completely eliminated while the crystallization could be avoided [3, 11]. More importantly, annealing at this temperature can make the bioactive glass 70S30C possess the maximum bioactivity [3]. For nanoindentation measurement, the electrospun scaffolds were firstly ground by hand for several minutes and then pressed into a mould to form column sample. The relative density of such samples is about 80%.

The X-ray diffraction (XRD) analysis of submicron bioactive glass fibers was conducted on a Philips X'pert PRO X-ray diffractometer with Cu (Kα) radiation. An energy disperse spectroscopy (EDS) analysis (Oxford INCA) was carried out to get the atomic proportion of Si and Ca elements in the scaffold. The chemical analysis of the electrospun submicron fibers was conducted with Fourier transform infrared (FT-IR) spectrometer in a Nicolet Nexus operating in transmission mode.

The morphology of the electrospun submicron fibers were characterized by field emission scanning electron microscope (FESEM, Sirion 200 FEG and Hitachi S4800), after the specimens were mounted on aluminum stubs and sputter-coated with palladium. The diameter of the submicron fibers was determined as an average over the values of arbitrarily selected fibers using high-magnification SEM images. The pore structure of the samples was analyzed using both SEM and N_2 gas adsorption (ASAP 2020 M + C). The porosity of the scaffold is calculated by dividing its apparent density ($\rho_{scaffold}$) by the density of the solid composite (ρ_{solid}):

$$\text{Porosity} = 1 - \frac{\rho_{scaffold}}{\rho_{solid}},$$

where $\rho_{scaffold} = \frac{\text{Mass of electrospun matrix (g)}}{\text{Volume of scaffold(cm}^3\text{)}}$, ρ_{solid} is 2.863 g/cm^3 as reported elsewhere [23]. Measurement results are averaged over four samples.

Nanoindentation measurements were carried out using a nano-indentation system (nanoindenter XP) at room temperature with a Berkovich diamond indenter. The tests were run at a constant strain rate of 0.05 s^{-1} with a continuous stiffness measurement option. As the nanoindenter tip approached the maximum penetration depth, the load was held constant for 10 s to stabilize the creep possibly occurred in the material. The depth limit of all the measurements was 2500 nm. The Poisson's ratio was about 0.18.

3 Results and discussion

The SEM micrographs of 70S30C submicron fibrous mat electrospun with the optimized parameters (sol concentration: 13% and applied voltage: 14 kV) were shown in Fig. 1a–c at different magnification. The three-dimensional fibrous mesh consists of interconnected fibers. It can be seen that the thickest fiber has a diameter of about 800 nm and the thinnest fiber has a diameter of about 50 nm, as shown in Fig. 1b, but the diameter of the most fibers is about 300 nm, as shown in Fig. 1b, c. The macroporous structure of the scaffold can be clearly seen from Fig. 1a, b, where the largest pore size can reach 10 μm. The rough surface of the fiber is shown in Fig. 1d, which will further increase the surface area of the fibers. The porosity calculated from the apparent density measurements of four samples was about 89.7%, indicating a highly porous structure of the fibrous scaffold.

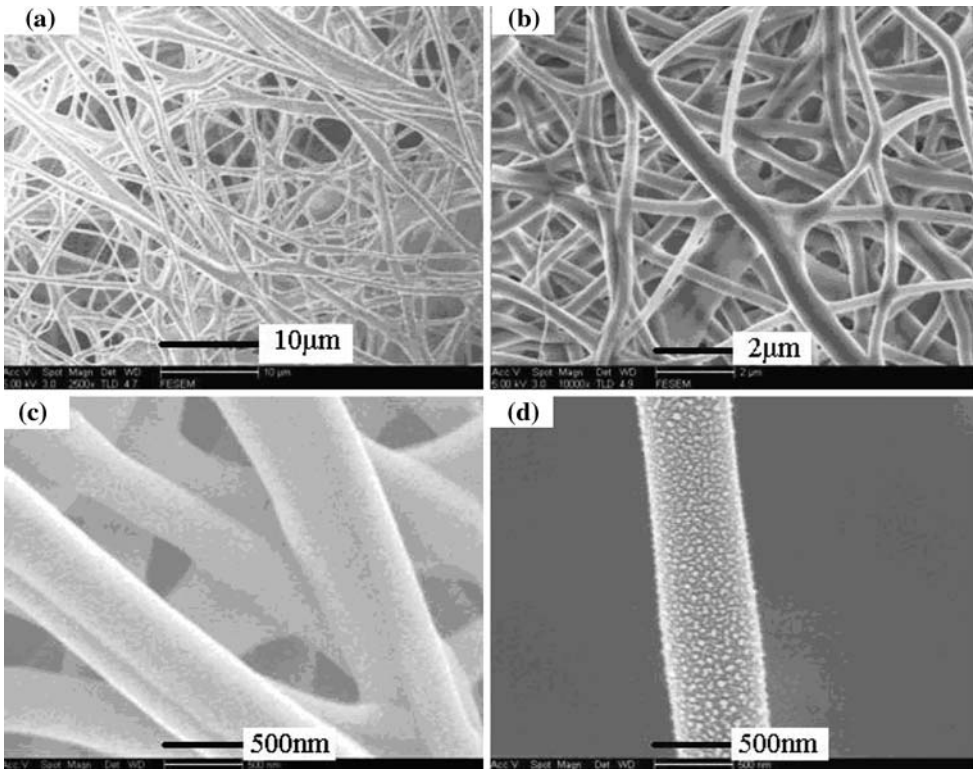

Fig. 1 Typical SEM images of electrospun submicron bioactive glass 70S30C fibers at different magnification (**a**–**c**), and the SEM image of a single fiber (**d**)

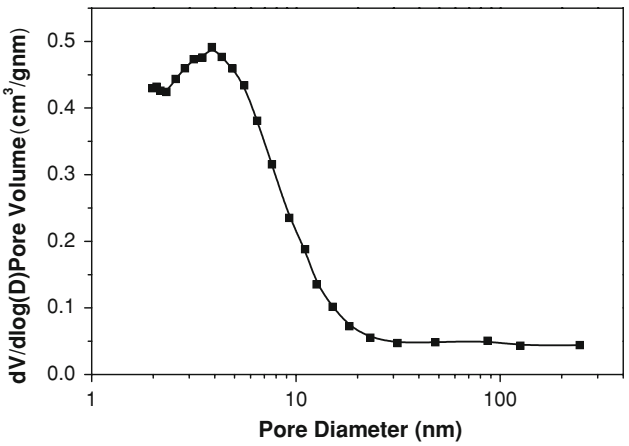

Fig. 2 Textural pore size distribution of submicron bioactive glass 70S30C mats, obtained from BJH analysis of N_2 sorption

Figure 2 shows the size distribution of mesopores obtained from N_2 adsorption isotherms using BJH analysis. The vertical axis is a derivative of the volume of nitrogen adsorbed into the surface of the bioactive glass scaffold at each pore diameter. The textural characteristics of mesopores in 70S30C scaffolds prepared with different method are presented in Table 1. The average diameter of the mesopores in the present electrospun 70S30C scaffolds is about 4.75 nm while the specific surface area and the total volume of the mesopores are 42.2 m^2/g and 0.039 cm^3/g, respectively, which is comparative to those in sol–gel derived 70S30C glass foam [3] but much smaller than those in 70S30C Gel–glass powder [9] and monolith [12]. The presence of mesopores is consistent with the rough surface of the electrospun fibers, as shown in Fig. 1d. As pointed out in Refs. [24, 25], the high porosity and large pore size of the fibrous scaffolds is beneficial for the cells to penetrate into the inner side of the scaffolds and the highly porous microstructure with interconnected pores is conducive to tissue ingrowth. Therefore the presence of both macropores and mesopores will make such electrospun 70S30C bioactive glass scaffold a good candidate for use in tissue engineering.

The XRD spectrum shown in Fig. 3 illustrates that the fibrous mats calcined at 600°C for 5 h are amorphous. The energy dispersive spectroscopy (EDS) profile of the fibers reveals that the composition of the glass is stoichiometric in the form of $70SiO_2 30CaO$, as shown in Fig. 4.

FTIR spectrum of the submicron fibers is illustrated in Fig. 5. In the spectrum the absorption bands near 450 and 578 cm^{-1} can be attributed to the Si–O–Si bending vibration, while the bands near 800 and 1070 cm^{-1} to the Si–O–Si symmetric and asymmetric stretching vibration, respectively [26]. Skipper et al. [27] have shown that calcium is loosely bound within the glass network and discerned Ca–O environment in the complex 70S30C

Table 1 Average diameter, surface area and volume of mesopores for electrospun 70S30C scaffold and sol–gel derived glass foam [3], gel–glass powder [9], gel–glass monolith [12] with the same composition of 70S30C

Samples	Average diameter (nm)	Surface area (m^2/g)	Volume (cm^3/g)
Electrospun 70S30C scaffold	4.75	42.2	0.039
Sol–gel derived 70S30C glass foam	1.0–17.5	12.8–122.7	–
70S30C gel–glass powder	20.4	75	0.38
70S30C gel–glass monolith	20.99 ± 0.55	135.87 ± 7.05	0.713 ± 0.033

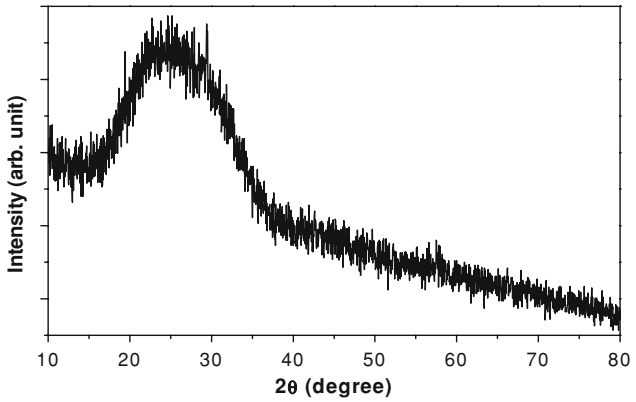

Fig. 3 XRD pattern of submicron bioactive glass 70S30C fibers calcined at 600°C for 5 h

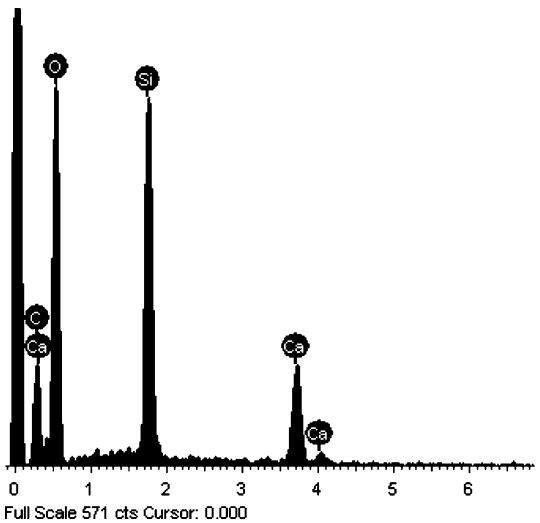

Fig. 4 EDS mapping of electrospun submicron bioactive glass 70S30C fibers

bioactive glass materials using neutron diffraction with isotopic substitution (NDIS) technique. The absence of Si–Ca bonds indicates that the glass is just a mixture of silica and calcia.

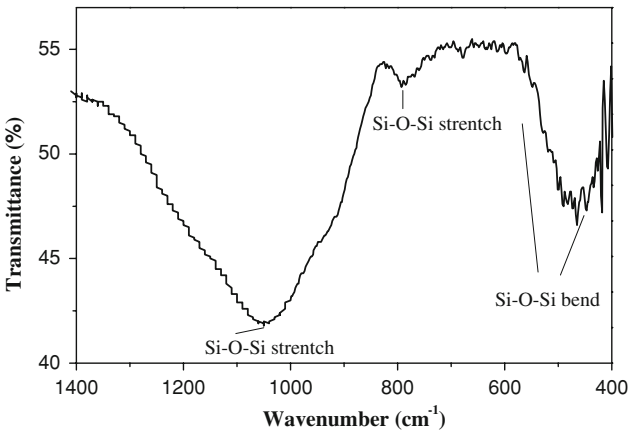

Fig. 5 FTIR spectrum of submicron bioactive glass 70S30C fibers calcined at 600°C for 5 h

It was already reported that solution concentration strongly affects fiber size while the spinning voltage is strongly correlated with the formation of bead defects in the fibers [28, 29]. At relatively low concentrations, finer fibers are obtained, but the number of beads in the fibers increases. During the electrospinning process, changing the applied voltage is an easily adjustable electrospinning parameter to control the morphology of fibers. The effect of the applied voltage on the morphology of bead defects in the fibers was studied in the range of 7–19 kV with solution concentration of about 9.5 wt.%, since steady jet can not occur at a voltage lower than 7 kV. From the morphology of the electrospun submicron fibers shown in Fig. 6, it can be seen that at a voltage of 7 kV a few small bead defects appear in the fibers. Both the density and size of the bead defects increase monotonously with the increasing voltage, since increasing the voltage causes the spinning jet less stable, which was in qualitative agreement with the results reported by Deitzel et al. [28]. The results indicate that adjusting the voltage to a relatively low value tends to decrease the bead defect density in the electrospun fibers.

Researches suggested that the elastic properties of materials at the micro structural level may be very different from those measured in macroscopic test [30].

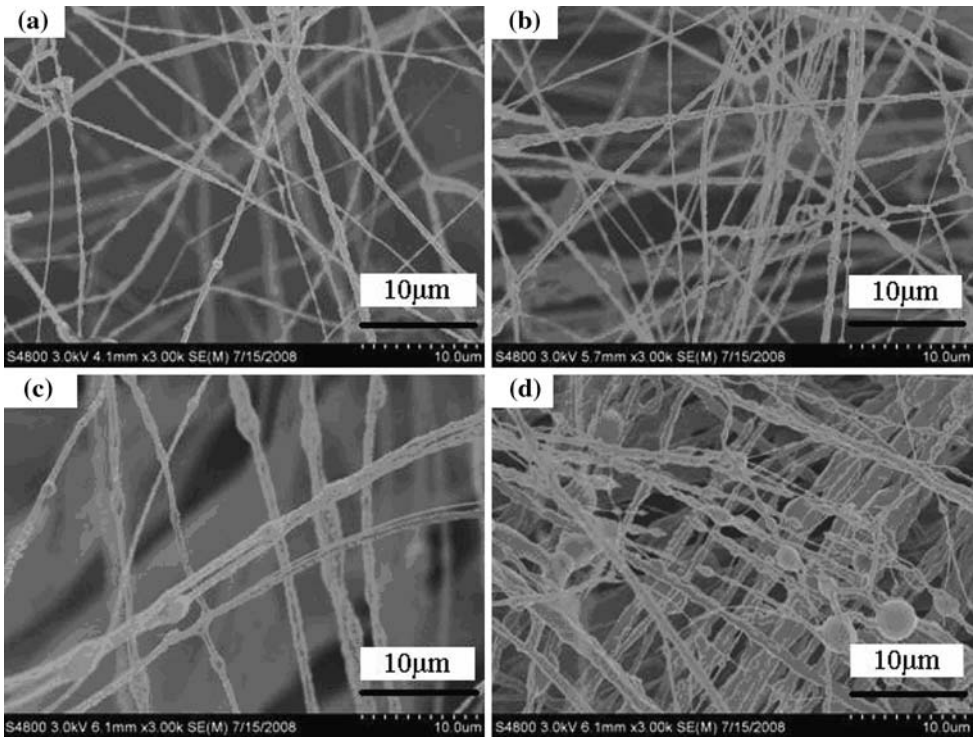

Fig. 6 Effect of the applied voltage on the morphology of bead defects in the submicron bioactive glass 70S30C fibers: **a** 7 kV; **b** 11 kV; **c** 15 kV; **d** 19 kV

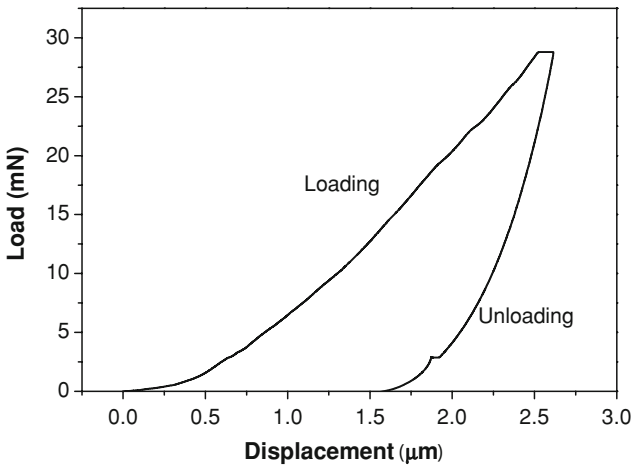

Fig. 7 Load-displacement curve of submicron bioactive glass 70S30C fibers, measured by nanoindentation

Nanoindentation is a powerful technique for the measurement of mechanical properties in diverse biomaterials, which has been proven to be useful in measurement of mechanical properties that are nearly impossible to assess through bulk testing [31]. It uses the recorded depth of penetration of an indenter into the specimen along with the measured applied load to determine the hardness of the test specimen. Elastic modulus and many other mechanical properties can also be obtained from the experimental load–displacement curve [32]. However, only a few nanoindentation studies have been reported for tissue scaffolds to date, and especially, nanoindentation studies on bioactive glass were seldom reported.

Figure 7 shows an example of the load-displacement curve for bioactive glass tested by nanoindentation. From such curves the elastic modulus and hardness can be obtained as 5.5 GPa and 0.21 GPa, respectively. Table 2 lists the micromechanical properties of several materials relative to bone or bone repair materials, tested by nanoindentation. Comparing with the other bone repair materials (Strontium-containing hydroxyapatite cement [33] and Hand-mixed Cemex®XL cement [34]), the elastic modulus of the present scaffold was higher and closer to the bone. The measured mechanical properties illustrate that this bioactive glass scaffold may be suitable for bone tissue engineering.

4 Conclusion

Bioactive glass 70S30C submicron fibers were synthesized by the electrospinning technique. The fibrous scaffolds possess large surface area, high porosity and well interconnected pore network structure. The diameters of submicron fibers were in the range of 50–800 nm. The hardness and elastic modulus of 70S30C fibers were measured by nanoindentation as 0.21 GPa and 5.5 GPa, respectively. In comparison with other bone scaffolds, the present fibrous scaffolds exhibit higher elastic modulus. These results imply that the electrospun submicron

Table 2 Micromechanical properties of bone [30] and bone repair materials: Strontium-containing hydroxyapatite cement [33] and Hand-mixed Cemex^{R}XL cement [34], tested by nanoindentation

Samples	Elastic Modulus, GPa (SD*)	Hardness, GPa (SD)
Cortical bone (Osteons)	22.4 (1.2)	0.617 (0.039)
Cortical bone (Interstitial lamellae)	25.7 (1.0)	0.736 (0.044)
Trabecular bone (Longitudinal)	19.4 (2.3)	0.618 (0.061)
Trabecular bone (Transverse)	15.0 (2.5)	0.515 (0.082)
Electrospun 70S30C bioactive glass	5.5 (0.8)	0.21 (0.04)
Strontium-containing hydroxyapatite cement	3.6 (0.3)	0.2391 (0.0304)
Hand-mixed Cemex®XL cement	2.76 (0.51)	0.170 (0.025)

* Standard deviations are shown in parentheses (SD)

bioactive glass fibers 70S30C may act as candidates of bone scaffolds.

Acknowledgement The authors thank Dr. Q. Liu at Ningbo Institute of Materials Technology & Engineering for the hardness measurement.

References

1. W.J. Boyle, W.S. Simonet, D.L. Lacey, Nature **423**, 337 (2003). doi:10.1038/nature01658
2. R. Murugan, S. Ramakrishna, Compos. Sci. Technol. **65**, 2385 (2005). doi:10.1016/j.compscitech.2005.07.022
3. J.R. Jones, L.M. Ehrenfried, L.L. Hench, Biomaterials **27**, 964 (2006). doi:10.1016/j.biomaterials.2005.07.017
4. K.J.L. Burg, S. Porter, J.F. Kellam, Biomaterials **21**, 2347 (2000). doi:10.1016/S0142-9612(00)00102-2
5. L.L. Hench, J.M. Polak, Science **295**, 1014 (2002). doi:10.1126/science.1067404
6. L.L. Hench, J. Mater. Sci. Mater. Med. **17**, 967 (2006). doi:10.1007/s10856-006-0432-z
7. P. Saravanapavan, L.L. Hench, J. Biomed. Mater. Res. **54**, 608 (2001). doi:10.1002/1097-4636(20010315)54:4<608::AID-JBM180>3.0.CO;2-U
8. J.R. Jones, O. Tsigkou, E.E. Coates, M.M. Stevens, J.M. Polak, L.L. Hench, Biomaterials **28**, 1653 (2007). doi:10.1016/j.biomaterials.2006.11.022
9. P. Saravanapavan, J.R. Jones, R.S. Pryce, L.L. Hench, J. Biomed. Mater. Res. **66A**, 110 (2003). doi:10.1002/jbm.a.10532
10. P. Saravanapavan, J.R. Jones, S. Verrier, R. Beilby, V.J. Shirtliff, L.L. Hench, J.M. Polak, Biomed. Mater. Eng. **14**, 467 (2004)
11. P. Saravanapavan, L.L. Hench, J. Non-Cryst. Solids **318**, 1 (2003). doi:10.1016/S0022-3093(02)01864-1
12. P. Saravanapavan, L.L. Hench, J. Non-Cryst. Solids **318**, 14 (2003). doi:10.1016/S0022-3093(02)01882-3
13. J.R. Jones, L.L. Hench, J. Mater. Sci. **38**, 3783 (2003). doi:10.1023/A:1025988301542
14. M.M. Pereira, J.R. Jones, L.L. Hench, Adv. Appl. Ceram **104**, 35 (2005). doi:10.1179/174367605225011034
15. C.Y. Xu, R. Inai, M. Kotaki, S. Ramakrishna, Biomaterials **25**, 877 (2004). doi:10.1016/S0142-9612(03)00593-3
16. H.-W. Kim, H.-E. Kim, J.C. Knowles, Adv. Funct. Mater **16**, 1529 (2006). doi:10.1002/adfm.200500750
17. W. Xia, D. Zhang, J. Chang, Nanotechnology **18**, 135601 (2007). doi:10.1088/0957-4484/18/13/135601
18. H.-W. Kim, H.-H. Lee, G.-S. Chun, J. Biomed. Mater. Res. **85A**, 651 (2008). doi:10.1002/jbm.a.31339
19. J. Venugopal, S. Low, A.T. Choon, T.S. Sampath Kumar, S. Ramakrishna, J. Mater. Sci. Mater. Med. **19**, 2039 (2008). doi:10.1007/s10856-007-3289-x
20. J.-H. Song, B.-H. Yoon, H.-E. Kim, H.-W. Kim, J. Biomed. Mater. Res. **84A**, 875 (2008). doi:10.1002/jbm.a.31330
21. D. Li, Y. Xia, Adv. Mater **16**, 1151 (2004). doi:10.1002/adma.200400719
22. S. Srouji, T. Kizhner, E. Suss-Tobi, E. Livne, E. Zussman, J. Mater. Sci. Mater. Med. **19**, 1249 (2008). doi:10.1007/s10856-007-3218-z
23. L.J. Skipper, F.E. Sowrey, D.M. Pickup, V. Fitzgerald, R. Rashid, K.O. Drake, Z. Lin, P. Saravanapavan, L.L. Hench, M.E. Smith, R.J. Newport, J. Biomed. Mater. Res. **70A**, 354 (2004). doi:10.1002/jbm.a.30093
24. K. Sombatmankhong, N. Sanchavanakit, P. Pavasant, P. Supaphol, Polymer (Guildf) **48**, 1419 (2007). doi:10.1016/j.polymer.2007.01.014
25. H. Yoshimoto, Y.M. Shin, H. Terai, J.P. Vacanti, Biomaterials **24**, 2077 (2003). doi:10.1016/S0142-9612(02)00635-X
26. R.M. Almeida, C.G. Pantano, J. Appl. Phys **68**, 4225 (1990). doi:10.1063/1.346213
27. L.J. Skipper, F.E. Sowrey, D.M. Pickup, K.O. Drake, M.E. Smith, P. Saravanapavan, L.L. Hench, R.J. Newport, J. Mater. Chem. **15**, 2369 (2005). doi:10.1039/b501496d
28. J.M. Deitzel, J. Kleinmeyer, J.D. Harris, N.C. Beck Tan, Polymer (Guildf) **42**, 261 (2001). doi:10.1016/S0032-3861(00)00250-0
29. S.-H. Tan, R. Inai, M. Kotaki, S. Ramakrishna, Polymer (Guildf) **46**, 6128 (2005). doi:10.1016/j.polymer.2005.05.068
30. J.-Y. Rho, M.E. Roy II, T.Y. Tsui, G.M. Pharr, J. Biomed. Mater. Res. **45**, 48 (1999). doi:10.1002/(SICI)1097-4636(199904)45:1<48::AID-JBM7>3.0.CO;2-5
31. D.M. Ebenstein, L.A. Pruitt, Nanotoday **1**, 26 (2006)
32. A.C. Fischer-Cripps, Surf. Coat. Tech. **200**, 4153 (2006). doi:10.1016/j.surfcoat.2005.03.018
33. G.X. Ni, Y.S. Choy, W.W. Lu, A.H.W. Ngan, K.Y. Chiu, Z.Y. Li, B. Tang, K.D.K. Luk, Biomaterials **27**, 1963 (2006). doi:10.1016/j.biomaterials.2005.09.044
34. G. Lewis, J. Xu, N. Dunne, C. Daly, J. Orr, J. Biomed. Mater. Res. Part B Appl. Biomater. **78B**, 312 (2006). doi:10.1002/jbm.b.30489